2.5

A COMPARISON OF HAZARD AREA PREDICTIONS BASED ON THE ENSEMBLE-MEAN PLUME VERSUS INDIVIDUAL PLUME REALIZATIONS USING DIFFERENT TOXIC LOAD MODELS

Christopher Czech[1], Nathan Platt[2] *, Jeffry Urban[2], Paul Bieringer[3], George Bieberbach[3], Andrzej Wyszogrodzki[3] and Jeffrey Weil[3]

[1]Clemson University, Clemson, SC

[2]Institute for Defense Analyses, Alexandria, VA

[3]National Center for Atmospheric Research, Boulder, CO

1. INTRODUCTION

There is anecdotal evidence that atmospheric transport and dispersion (AT&D) models greatly over-predict the consequences of large scale toxic industrial chemical releases (Urban et al., 2010 and Sommerville et al., 2009). This evidence is largely based on a comparison between the observed locations of human or animal casualties (or lack thereof) resulting from chlorine rail car accidents and the hazard area for lethal effects derived from AT&D model predictions. There are a number of potential reason for these discrepancies, which include: (1) inaccurate descriptions of the input parameters needed to run AT&D models, such as source term descriptions and meteorology; (2) the potential inability of AT&D models to capture some important features associated with the propagation of a large volume of dense vapor; and (3) inaccurate consequence estimation models, including potential inaccuracies in the in toxicity parameters or in the toxicity models used to estimate toxic inhalation effects. This work concentrates on the consequence estimation methodology, specifically on a toxic load modeling of the assessment of casualties. The details of the toxic load models used in this paper will be presented in the next section. In particular, we have investigated (1) the difference between the toxic load hazard area calculated directly from the ensemble mean plume and the ensemble mean of toxic load hazard areas calculated from individual plume realizations (ensemble members), and (2) the difference between toxic load hazard areas computed using different toxicity models that express a generalized toxic load.

The most common way for an AT&D model to calculate toxic effects is based on the total inhaled dose. These effects are independent of the manner in which this dose was accumulated (i.e., they are independent of the exposure history). But for many chemicals, it has been observed that the time dependence of the exposure is important – for instance, inhaling a dose of chlorine over a short period of time has much stronger effects than inhaling the same dose over an extended period of time (ten Berge et al., 1986 and Sommerville et al., 2009). Toxic load modeling tries to account for this effect by utilizing the toxic load exponent n (approximately equal to 2.75 for chlorine) (Sommerville et al., 2009), which will be defined later. While the experimental data supporting toxic load modeling were derived using concentration exposure profiles in the form of a rectangular pulse, the actual exposures from hazardous plumes are not well-described by rectangular pulses. There are several proposed generalizations of the toxic load model to the case of time-varying concentration, none of which have been validated using animal experiments. In this work, a total of four toxic load models are considered that cover the full spectrum of conservatism in casualty and hazard area estimation.

The majority of AT&D models presently used for consequence assessment predict a “mean” plume that approximates the ensemble average over a large number of plume realizations. In a number of studies, toxic load modeling is applied to the concentration output of these models to produce casualty estimates. Additionally, the few AT&D models that apply toxic load modeling internally use the ensemble average plume (some models may also include statistical estimates of the variance of the ensemble average, e.g. Sykes et al., 2007). By its definition, the “mean” plume “smears out”, in both time and space, the high concentration regimes that would be expected within individual plume realizations. The question arises whether the casualties estimated from the “mean plume” could differ from the mean of the casualties estimated from individual plume realizations when using toxicity models that depend on the time history of the exposure, such as toxic load models.

*Corresponding author address: Nathan Platt, Institute for Defense Analyses, 4850 Mark Center Drive, Alexandria, VA 22311-1882; e-mail: nplatt@ida.org.

The National Center for Atmospheric Research (NCAR) Virtual Threat Response Emulation Test Bed (VTHREAT) modeling system is a suite of models designed to provide a virtual environment for meteorological modeling and AT&D modeling. It includes an Eulerian semi-Lagrangian model for geophysical flows (EULAG) that utilizes a Large Eddy Simulation (LES) numerical technique coupled with a Lagrangian Particle Dispersion Model (LPDM) (Bieberbach et al., 2010). A key feature of VTHREAT is its potential to produce realistic, statistically representative hazardous materials plumes that include turbulence-induced fluctuating and meandering components. VTHREAT actually predicts individual realizations of the plume and not a "mean" plume.

We are assisting with the validation of VTHREAT; as part of this work, we have obtained a high resolution (in space and time) set of predictions that contains 20 plume realizations for a continuous release of a neutral-buoyancy tracer gas over flat terrain under stable atmospheric conditions. This data set is an ideal candidate for comparing toxic load calculations based on a "mean" plume with calculations based on individual plume realizations in order to assess the potential effect on casualty estimation.

This paper is organized as follows: Section 2 briefly describes toxic load modeling and its extension to time-dependent exposure profiles; Section 3 briefly describes VTHREAT, a set of plume realizations produced by VTHREAT, and the construction of an approximate ensemble average plume; Section 4 describes metrics that were used in the analysis; Section 5 presents the preliminary results of the analysis; and Section 6 provides conclusions and a discussion of future work.

2. HABER'S LAW AND TOXIC LOAD MODELING

Different models have been proposed to relate a chemical concentration exposure profile to the toxic effect on humans. A common assumption is that toxic effects are a function of only the total inhaled dosage. This relationship between exposure and toxic response is called Haber's law, which can be written as follows

$$D(\mathbf{x}) = C(\mathbf{x})T \tag{1}$$

where $D(\mathbf{x})$ denotes the dosage at a location $\mathbf{x}$ and $C(\mathbf{x})$ is a steady concentration to which a subject located at point $\mathbf{x}$ is exposed over a duration T. According to Haber's law, the two notional concentration profiles depicted in Figure 1 both result in the same toxic effect as long as the total dosage is the same, regardless of whether the dosage is delivered via a long exposure to a low concentration or a short exposure to a high concentration. While the original Haber's law was defined for constant concentration only, a simple extension of Haber's law to a non-steady time-varying concentration $c(\mathbf{x},t)$ is quite prevalent (Sommerville et al., 2006):

$$D(\mathbf{x}) = \int c(\mathbf{x},t)dt \tag{2}$$

In this formulation, the limits of integration are irrelevant as long as they capture the entire passage of the hazardous plume at spatial location $\mathbf{x}$. We note that when Haber's Law is assumed, toxic effects are independent of the manner in which the dosage is accumulated.

For any given level of exposure, there is a need to estimate effects of such an exposure. While individual subjects might respond differently to the same dosage exposure, it is possible to use simple probabilistic notions to characterize overall subject group response when exposed to specific dosage – for instance what is the average number of healthy young soldiers that would be incapacitated when exposed to a prescribed dosage of a particular chemical. The typical model for consequence assessment used to estimate toxicological effects is a probit model based on a log-normal distribution described by two-parameters: the median effective dosage Eff_{50} and the probit slope. Eff_{50} corresponds to the dosage that is required to achieve a certain effect (e.g., death, incapacitation, etc.) in 50% of the population. To determine Eff_{50} and the probit slope, one typically needs to perform animal experiments to determine the dosage at which the specified toxicological effects occur; these results are then extrapolated to the human population. Typical studies involve exposing a number of animal subjects in a sealed chamber to constant concentrations of a toxic chemical over different time intervals (notionally denoted in Figure 1) and recording the fraction of the population that shows particular toxic effects.

Early in the study of chemical toxicity it was observed that Haber's law does not hold for all chemical agents, including several chemical warfare agents. Some authors have suggested that for these chemicals the population response is better described by a log-normal function of the "toxic load" than of the dosage, where the toxic load is defined as:

$$TL(\mathbf{x}) = C^n(\mathbf{x})T = (C(\mathbf{x})T)^n T^{1-n} = D^n(\mathbf{x})T^{1-n} \quad (3)$$

Here, *n* is the "toxic load exponent", which, like the other toxicity parameters, is determined by fitting the available experimental exposure-response data. For the two notional concentration profiles depicted in Figure 1, if *n* > 1, an exposure to a short-duration but high-concentration pulse produces stronger toxic effects than an exposure to a long-duration but low-concentration pulse. The toxic load model reduces to Haber's law when *n* = 1. As is the case with Haber's law, the toxic load model requires two additional parameters to estimate the fraction of the population exhibiting a particular toxic effect (e.g., death, incapacitation, etc.), such as the "median effective toxic load" and the corresponding probit slope. We note that the toxicity parameters associated with the use of a toxic load model may not equal the ones that apply when Haber's Law is assumed.

As is the case for Haber's law, the experimental basis for the toxic load model is derived based on constant concentration exposure only. In actuality, real-life exposures may vary in time, as notionally depicted in Figure 2. In addition, even simple AT&D models used in consequence assessment today produce time-varying concentration profiles. Thus, there is a need to extend the toxic load model described in Eq. 3 to non-steady exposures. Several such extensions have been proposed, but none have been validated experimentally.

In this paper we consider four possible extensions of the toxic load model to the case of time-varying exposures, which are briefly described below. All of these models reduce to Eq. 3 in the limit of a steady exposure over a finite duration.

Average Concentration Toxic Load Model

One natural extension of the toxic load model to the case of time-varying exposures is to replace the steady concentration in Eq. 3 with the average concentration over the exposure duration *T* (Hilderman et al., 1999):

$$TL_{AverConc}(\mathbf{x}) = \left(\frac{\int c(\mathbf{x},t)dt}{T}\right)^n T = D^n(\mathbf{x})T^{1-n} \quad (4)$$

where $D(\mathbf{x})$ denotes the total dosage accumulated at location **x** over duration *T*. Since Gaussian puff or plume models generally predict exposures that asymptotically decrease to zero concentration over infinite time, a low-level concentration threshold may be used to determine the plume arrival and departure times to calculate the effective plume duration *T*.

Integrated Concentration Toxic Load Model

Another extension of the original toxic load model, which we call the integrated concentration toxic load model, was proposed by ten Berge and van Heemst, 1983:

$$TL_{Integrated.}(\mathbf{x}) = \int c^n(\mathbf{x},t)dt \quad (5)$$

This model extends Eq. 3 to the case of time-varying concentrations by employing a time integral over the instantaneous concentration raised to the power of the toxic load exponent. The integrated concentration toxic load model appears to be the most common extension of Eq. 3 used for consequence estimation within the AT&D modeling community.

Concentration Intensity Toxic Load Model

While being conceptually simple and elegant, the integrated concentration toxic load model requires rather intensive computational power to calculate hazard areas or estimate casualties (Sommerville et al., 2006). Both of these calculations require the calculation of toxic load values at a large number of locations. Most AT&D models used for hazard assessment already calculate dosages according to Eq. 2. Thus, there is an interest to develop methodologies that simplify the calculation of toxic load values at a large number of locations. The Hazard Prediction Assessment Capability (HPAC) model developed and maintained by the Defense Threat Reduction Agency (DTRA) is capable of calculating not only the integrated concentration (dosage) at a large number of locations, but also the concentration variance. HPAC uses these two quantities to calculate a toxic load (Sykes et al., 2007). While HPAC's methodology is applicable to the ensemble-averaged concentration and its variance, it needs to be modified to be applied to individual realizations of the concentration field. We have adapted this methodology for use with the individual realizations of the concentration field obtained from VTHREAT as follows:

$$TL_{ConcIntens}(\mathbf{x}) = D^n(\mathbf{x}) T^{1-n}_{ConcIntens}(\mathbf{x})$$
$$T_{ConcIntens}(\mathbf{x}) = \frac{\left(\int c(\mathbf{x},t)dt\right)^2}{\int c^2(\mathbf{x},t)dt} = \frac{D^2(\mathbf{x})}{\int c^2(\mathbf{x},t)dt} \quad (5)$$

Here $c(\mathbf{x},t)$ can represent either an individual concentration field or the ensemble average concentration field, depending on whether the toxic load is being calculated for an individual realization of the plume or for the ensemble-averaged plume. The quantity $T_{ConcIntens}(\mathbf{x})$ is sometimes called the generalized exposure duration. These equations can be combined together to yield the following expression for concentration intensity toxic load:

$$TL_{ConcIntenc}(\mathbf{x}) = \frac{D^{2-n}(\mathbf{x})}{\left(\int c^2(\mathbf{x},t)dt\right)^{1-n}} = \frac{\left(\int c(\mathbf{x},t)dt\right)^{2-n}}{\left(\int c^2(\mathbf{x},t)dt\right)^{1-n}} \quad (6)$$

Peak Concentration Toxic Load Model

Stage, 2004 proposed a method for the practical calculation of Acute Exposure Guideline Levels (AEGLs) for time-varying exposures that uses the principles of toxic load modeling. We have adapted it to the case of individual concentration realizations as follows. Let us define a generalized exposure time $T_{PeakConc}$ as

$$T_{PeakConc}(\mathbf{x}) = \frac{D(\mathbf{x})}{c_{Peak}(\mathbf{x})} = \frac{\int c(\mathbf{x},t)dt}{c_{Peak}(\mathbf{x})} \quad (7)$$

where $c_{Peak}(\mathbf{x})$ denotes the peak concentration observed at location $\mathbf{x}$ during the exposure interval. Then, the peak concentration toxic load model can be written as

$$TL_{PeakConc}(\mathbf{x}) = D^n(\mathbf{x}) T^{1-n}_{PeakConc}(\mathbf{x}) = \frac{D(\mathbf{x})}{c^{1-n}_{Peak}(\mathbf{x})} \quad (8)$$

Some Notes on Different Toxic Load Models

We first note that when the toxic load exponent n equals 1, all of the aforementioned toxic load models reduce to Haber's law.

It should be noted that for three of the toxic load models (Integrated Concentration, Concentration Intensity and Peak Concentration) it may be necessary to evaluate the toxic load using a concentration $c(\mathbf{x},t)$ that is time-averaged over a fast timescale to remove high-frequency concentration fluctuations. From a physiological perspective, it is unlikely that high-frequency concentration fluctuations that occur on a timescale faster than the time it takes to take a single breath of air would have a significant impact on human toxicity. Therefore, it may be necessary to apply a time-averaging of the concentration time series over a timescale on order of a few seconds before calculating the toxic load integrals. This may be accomplished numerically by replacing the integral with a sum over discrete timesteps. The toxic load calculated by this procedure could, in principle, significantly depend on the choice of averaging time (integration timestep) (Sommerville et al., 2006).

We would like to conclude this description of the toxic load models considered in this study with a few comments about the relative magnitude of the toxic loads derived by different models, which we have bounded in the case that the toxic load exponent n is greater than 1. In this case, the toxic load values resulting from the Average Concentration and Peak Concentration toxic load models most likely represent two extremes of conservatism in estimating the toxic load, with the Average Concentration model generating the lowest toxic load and the Peak Concentration model generating the highest toxic load, as notionally demonstrated in Figure 3. The brown line denotes a notional Gaussian concentration profile at some spatial location, the blue rectangle denotes an equivalent steady exposure profile in the Average Concentration toxic load model for this Gaussian-shaped concentration profile, and the green rectangle denotes an equivalent steady exposure profile used in the Peak Concentration toxic load model. The time integrals of the exposure profiles (e.g., the areas under the curve) are the same in each case, but the toxic load calculated using the Average Concentration model are not larger than those calculated using the Peak Concentration model when $n > 1$. In fact, it can be shown that for any time-dependent exposure, the following relationship always holds when $n > 1$:

$$TL_{AverConc} \le \left\{TL_{Integrated}, TL_{ConcInten}\right\} \le TL_{PeakConc} \quad (9)$$

3. VTHREAT PREDICTIONS OF INDIVIDUAL PLUME REALIZATIONS

The National Center for Atmospheric Research (NCAR) Virtual THreat Response Emulation and Analysis Testbed (VTHREAT) modeling system is a

suite of models designed to provide a virtual Chemical, Biological, Radiological and Nuclear (CBRN) release environment. It includes an Eulerian semi-Lagrangian model for geophysical flows (EULAG) that utilizes a Large Eddy Simulation (LES) numerical technqiue coupled with a Lagrangian Particle Dispersion Model (LPDM) (Bieberbach et al., 2010). This tool has the potential to support a wide range of analyses including: (1) the development, test, and evaluation of chemical-biological defense and meteorological sensors, algorithms, and architectures; (2) acquisition studies (e.g., analyses of alternatives, trade-off studies); (3) the planning of AT&D field experiments and the evaluation of their results; and (4) the formulation and investigation of concepts of operation (e.g., rules governing the employment of protective measures in a battlefield environment).

VTHREAT components include virtual chemical, biological, and meteorological sensors as well as models of background levels of contaminants, such as particulates. A key feature of VTHREAT is its potential to produce realistic and representative meteorological fields and hazardous plumes that include fluctuating and meandering components. Two key quantities that VTHREAT is designed to simulate at multiple locations and times are: (1) the agent concentration (a scalar quantity), and (2) the wind velocity (a vector quantity). As part of our validation support of VTHREAT (Platt et al., 2010), VTHREAT was used to simulate Trial 54 from the Fusing Sensor Information from Observing Networks (FUSION) Field Trial 2007 (FFT 07) (Storwold, 2007). This highly instrumented test was conducted at the U.S. Army's Dugway Proving Ground (DPG) and was designed to collect data to support the further development of prototype source term estimation algorithms. Trial 54 involved the continuous release of propylene gas for 10 minutes from a single source. The trial took place in the early morning in the presence of a steady southerly wind. Subsequent re-analysis of the available meteorological data has suggested that the atmospheric boundary layer was undergoing a morning transition from stable conditions to either neutral or slightly unstable conditions.

VTHREAT was used to simulate 20 individual realizations of Trial 54. These realizations were produced at a 1 second temporal resolution and a 5 meter spatial resolution in all three dimensions. The simulation domain was approximately 800 meters wide by 1600 meters long by 500 meters high. Figure 4 shows a sample snapshot of the concentration field for one of the realizations at 500 seconds after the start of the release.

Two methods were used to estimate the ensemble mean plume, which is expected to correspond approximately to the hazardous plume produced by most AT&D models that are presently used for consequence assessment. The first method uses a straightforward average over 20 realizations at each point in space and time. Figure 5 shows a snapshot at 500 seconds after the start of the release of an ensemble mean plume estimated by this technique. Comparing Figures 4 and 5, we note that the snapshot of the estimated ensemble mean plume is much smoother than snapshots of individual realizations evaluated at the same time. Nevertheless, there remain significant variations in concentration within the ensemble mean plume even on a logarithmic concentration scale, which are probably caused by the limited number of realizations (20) used to estimate the ensemble average. To further smooth out the estimated ensemble mean plume in the hopes of better representing the average over a large number of ensemble members, we employed an additional 60-second running window time average of the concentration field after we constructed the ensemble average. Figure 6 shows a snapshot of the ensemble mean plume estimated by this technique.

We would like to conclude this section with the following note. For an actual release of hazardous material into atmosphere, individual people would be expected to be exposed to concentration realizations similar to the individual concentration realizations (including fluctuations) predicted by VTHREAT, and not to the ensemble-averaged plume produced by the majority of AT&D models in use today.

4. COMPARISON METRICS

For each individual plume realization provided by VTHREAT we calculated the toxic load at each location in the concentration field using each of the four toxic load models discussed previously. Each of these toxic load fields can be considered as representing the spatial distribution of toxic loads that could be delivered to a population in a real-world event. We also calculated the toxic load at each location using the ensemble-averaged concentration field directly. This toxic load field is intended to represent the distribution of toxic loads that might be predicted by a Gaussian AT&D mode. Figure 7 shows example toxic load "plumes" calculated by these techniques using the Integrated Concentration toxic load model with n = 1.5. Figure 7a shows the toxic load field for an individual realization of the plume, while Figure 7b shows the toxic load field calculated the approximated ensemble average concentration field.

The following procedure was established to define a comparison metric:

1. Choose a threshold toxic load value.

2. Determine the area (in m^2) of the toxic load field that exceeds the threshold value at a given height above ground level.

3. Repeat this process for a predetermined set of threshold toxic load values.

4. Apply this process to the toxic load field calculated from the concentration field from each individual realization of a release. Also apply it to the toxic load field calculated from the ensemble-average concentration field.

We further illustrate the application of this procedure to individual plume realizations and the ensemble-averaged plume using two flowcharts, depicted in Figure 8. The procedure produces a set of "areas above threshold" as a function of different toxic load threshold values for each toxic load field that is considered. Figure 7 notionally demonstrates outcome of this procedure using a toxic load threshold of 8 mg^n-min-m^{-3n}. The resulting areas-above-threshold are shown at the bottom of the panels. Our metrics include not only the area-above-threshold values calculated for individual release realizations, but also the ratio of the area-above-threshold for each realization to the area-above-threshold for the toxic load calculated from the ensemble mean concentration. This ratio is a dimensionless quantity.

5. SUMMARY OF RESULTS

Three different toxic load exponents n = 1, 1.5 and 2.75 were used to calculate the two "area-above-threshold" metrics described previously for each of the four toxic load models. For n = 1 (when Haber's law applies), all four toxic load models agree with each other. Figure 9 shows the areas-above-threshold as a function of the toxic load threshold level. The "realization mean", denoted by black circles, corresponds to the average of the area values taken over the 20 individual realizations (ensemble members). Likewise, the "realization maximum" (maximum area observed among the 20 realizations) is denoted by light green diamonds and the "realization minimum" is denoted by light blue squares. The vertical black line denotes the span over which 90% (18 of 20) of the areas-above-threshold fall. The area-above-threshold values for the toxic load field calculated from the ensemble mean concentration are denoted by brown pluses. As expected for the Haber's Law regime (n = 1), the results of all four toxic load models agree with each other, and the ensemble average of toxic load areas agrees with the toxic load area calculated from the ensemble average concentration. Additionally, a wide spread in toxic load areas is seen among individual realizations, especially at the low toxic exposure levels. This indicates that there is a substantial statistical uncertainty in the area over which low-level toxic effects might be observed in a real-world event.

Figure 10 shows the areas-above-threshold as a function of toxic load threshold for n = 1.5. With the exception of the Average Concentration toxic load model, almost all individual release realizations have a larger toxic load area than the corresponding toxic load area calculated from the ensemble mean concentration field. Figure 11 is the same as Figure 10 except the individual areas-above-threshold have been normalized by dividing them by the area-above threshold for the toxic load field calculated from the ensemble mean concentration field. With the possible exception of the Average Concentration toxic load model, we conclude that for n = 1.5, the ratio of the average of toxic load area for individual plume realizations to the toxic load area calculated from the ensemble mean concentration increases as the toxic load threshold increases. Additionally, the spread in the aforementioned ratio also increases as the toxic load threshold increases.

Similar trends hold, and are even stronger, when toxic load exponent n = 2.75, as shown in Figures 12 and 13. Now, with the exception of the Average Concentration toxic load model, all realizations have a significantly larger toxic load area than the corresponding toxic load area calculated from the ensemble average concentration. Additionally, at the higher toxic load thresholds, both the Integrated Concentration and Concentration Intensity toxic load models significantly under-predict hazard areas (by up to a factor of 6) when the toxic load calculated from the ensemble average concentration is used compared to either the hazard areas calculated from individual realizations or to the average of hazard areas calculated from individual plume realizations.

We conclude this section by noting that two methods used to simulate the ensemble mean plume (e.g., point-to-point spatio-temporal averaging over 20 individual realizations versus the same procedure with an additional temporal 60-second running window averaging) do not substantially change the results discussed above. Figure 14 compares the sensitivity of the area ratio metric to the choice of ensemble averaging technique using the Integrated Concentration

and Concentration Intensity toxic load models with n = 1.5. At the lower toxic load thresholds the area ratios are almost indistinguishable from each other for both ensemble-averaging methods. At the higher toxic load thresholds, where the hazard areas are rather small and small differences in the estimated ensemble average plume could significantly amplify the area ratios, we note a larger discrepancy between calculated area ratios between the two ensemble-averaging methods. The overall trend, however, stays the same.

6. DISCUSSION AND FUTURE WORK

In this paper we briefly investigated the potential effects of the choice of toxic load model and the use of ensemble-average plumes derived from AT&D models in place of individual plume realizations on the estimation of the toxic effects resulting from the inhalation of hazardous chemicals. To do so we obtained 20 individual realizations of a notional plume simulated by the VTHREAT modeling system, numerically estimated the ensemble mean plume from these realizations using two methods, and then compared the areas exceeding particular toxic load thresholds obtained from this ensemble mean plume to the areas derived from applying toxic load modeling to individual plume realizations.

The original toxic load model was derived from and experimentally fitted to population response data obtained from exposures of animals to a steady concentration of a toxic chemical in a closed chamber. To the best of our knowledge there is no official (or experimentally validated) extension of the toxic load model to time-varying concentration fields. Thus, we considered a total of four proposed extensions of the toxic load model to time-varying concentrations. We call these the Average Concentration, Integrated Concentration, Concentration Intensity, and Peak Concentration toxic load models.

Our comparison metrics include the “area above threshold” for a set of notional toxic load values and the ratio of this area calculated using an individual plume realization to the area calculated using the ensemble average of plume realizations.

Our main conclusion is that great care should be exercised when toxic load modeling is used to calculate the human health consequences of a toxic release. Most AT&D models that are presently used for consequence assessment predict ensemble mean plumes, which tend to be smoother in both space and time than the turbulent plumes that may be observed in a real event. Toxic load modeling magnifies the effects of localized (both in space and time) concentration “hot zones” for chemicals that have a toxic load exponent greater than 1, resulting in hazard areas derived from ensemble mean plumes that are significantly smaller than those derived from typical plume realizations. At higher toxic load thresholds, for which the most severe effects (e.g., deaths) are expected, the ensemble mean plume could *greatly under-predict* hazard areas. As mentioned earlier, for an actual release of hazardous material into atmosphere, individual people would be expected to be exposed to concentration realizations similar to individual concentration realizations (including fluctuations) predicted by VTHREAT and not the ensemble averaged plume produced by the majority of AT&D models in use today.

Additionally, while not explicitly mentioned in this paper, different toxic load models could produce very different estimates of the toxic load exposure given the same concentration profile and, as a result, produce very different estimates of hazard areas. There is no experimental evidence to either validate or refute different extensions of the toxic load model extensions that account for time-varying concentrations, but there are many such extensions being advocated for consequence assessment or even being used for that purpose. Thus, there is a great need to institute a research program to try to establish the validity of the toxic load models that have been proposed or are being used.

We would like to conclude this paper on a cautionary note. The results presented here are still preliminary. The VTHREAT simulations involved 20 predictions of a single continuous release on a relatively small spatial scale. The release took place in the early morning under stable or neutral atmospheric conditions. Additionally, the threshold toxic load values used in the estimates of the hazard areas were not related to actual toxic endpoints. Also, with the exception of the Average Concentration toxic load model, none of the toxic load models we considered (as adapted for use with individual realizations of the concentration field) take into account concentration intermittency or repeated exposures. In the future we plan to consider both continuous and instantaneous releases under both stable and unstable (i.e.., convective) atmospheric conditions; consider additional toxic load models that deal with intermittency in the exposure profiles; and further investigate differences between various toxic load models.

ACKNOWLEDGMENTS

This effort was supported by the Defense Threat Reduction Agency with Dr. John Hannan as the project monitor. The authors would like to thank Dr. Alison Lawrence, Dr. Jeff Grotte, and Mr. Doug Schultz from the Institute for Defense Analyses for numerous fruitful discussions regarding this work. The views expressed in this paper are solely those of the authors.

REFERENCES

Bieberbach, G., Bieringer, P.E., Wyszogrodzki, A., Weil, J., Cabell, R., Hurst, J., and J. Hannan (2010). *Virtual chemical and biological (CB) agent data set generation to support the evaluation of CB contamination avoidance systems*, The Fifth Symposium on Computational Wind Engineering (CWE 2010), Chapel Hill, North Carolina.

Hilderman, T.L., Hrudle, S.E. and D.J. Wilson (1999). *A model for effective toxic load from fluctuating gas concentration,* Journal of Hazardous Materials, **64,** pp. 115-134.

Sommerville, D.R., Park, K.Y., Kierzewski, M.O., Dunkel, M.D., Hutton, M.I. and N.A. Pinto (2006). *Toxic Load Modeling*, in Inhalation Toxicology, Second Edition, edited by H. Salem and S.A. Katz, Boca Raton, FL, CRC Press, pp. 137-158.

Sommerville, D.R., Bray, J.J., Jablonski, R.E., Reutter-Christy, S.A. and E.E. Shelly (2009). *Review of Human Lethality Estimates for Chlorine Inhalation*, Presentation **J14.4** at the Eighth Symposium on the Urban Environment, 89th Annual American Meteorological Society Meeting, Phoenix, Arizona, January 2009

Stage, S.A. (2004). *Determination of Acute Exposure Guideline Levels in a Dispersion Model*, Journal of the Air & Waste Management Association, **54**, pp. 49–59.

Sykes, R.I., Parker, S.F., Henn, D.S., and B. Chowdhury (2007). *SCIPUFF Version 2.3 Technical Documentation*, L-3 Titan Technical Report.

ten Berge, W.F., and M.V. van Heemst (1983). *Validity and accuracy of a commonly used toxicity-assessment model in risk analysis*, Fourth International Symposium on Loss Prevention and Safety Promotion in Process Industries, Vol. 1, Institute of Chemical Engineers, Rugby, United Kingdom, pp. 11-112.

ten Berge, W.F., Zwart, A., and L.M. Appleman (1986). *Concentration-Time Mortality Response Relationship of Irritant and Systematically Acting Vapors and Gases*, Journal of Hazardous Materials 13, pp. 301-309

Urban, J.T., Platt, N., Adelizzi, E.A., Bucher, C.R., Henrikson, J.T., and K. Papadantonakis (2010). *Evaluation of Transport and Dispersion Modeling Tools for Chemical Facilities Terrorism Risk Assessment Applications: Final Report*, Institute for Defense Analyses Paper P-4605, prepared for the Chemical Security Analysis Center, U.S. Department of Homeland Security.

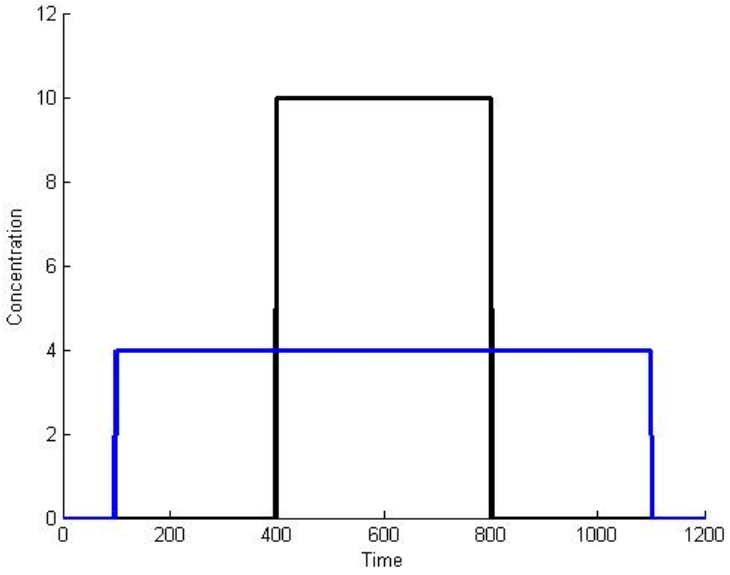

Figure 1. Two notional concentration profiles. Both profiles depicted in this picture have the same area under the curve and therefore would result in the same dosage for the exposure. If Haber's law applies, then the toxicological effects produced by exposure to either of these two concentration profiles would be the same. If a toxic load model with a toxic load exponent $n > 1$ applies, then the toxicological effects produced by exposure to the higher-concentration pulse are more severe than the toxicological effects produced by exposure to the lower-concentration pulse.

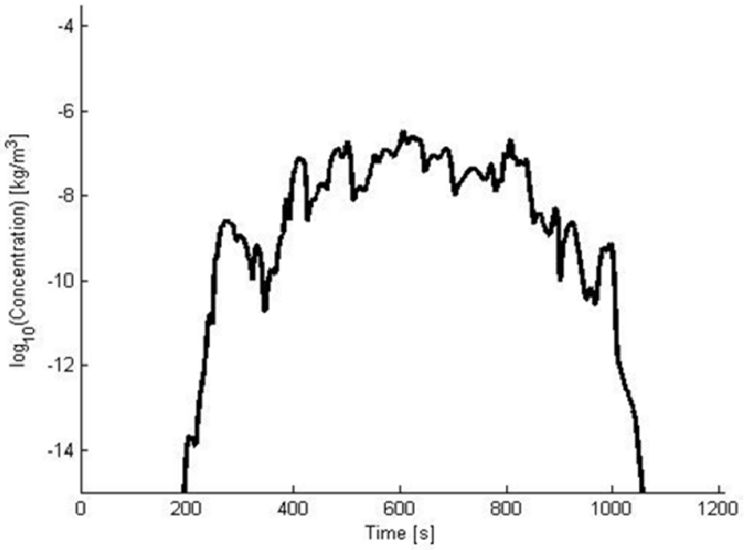

Figure 2. Notional chemical concentration profile that might be expected at a given location for a real-world exposure to an airborne hazardous material.

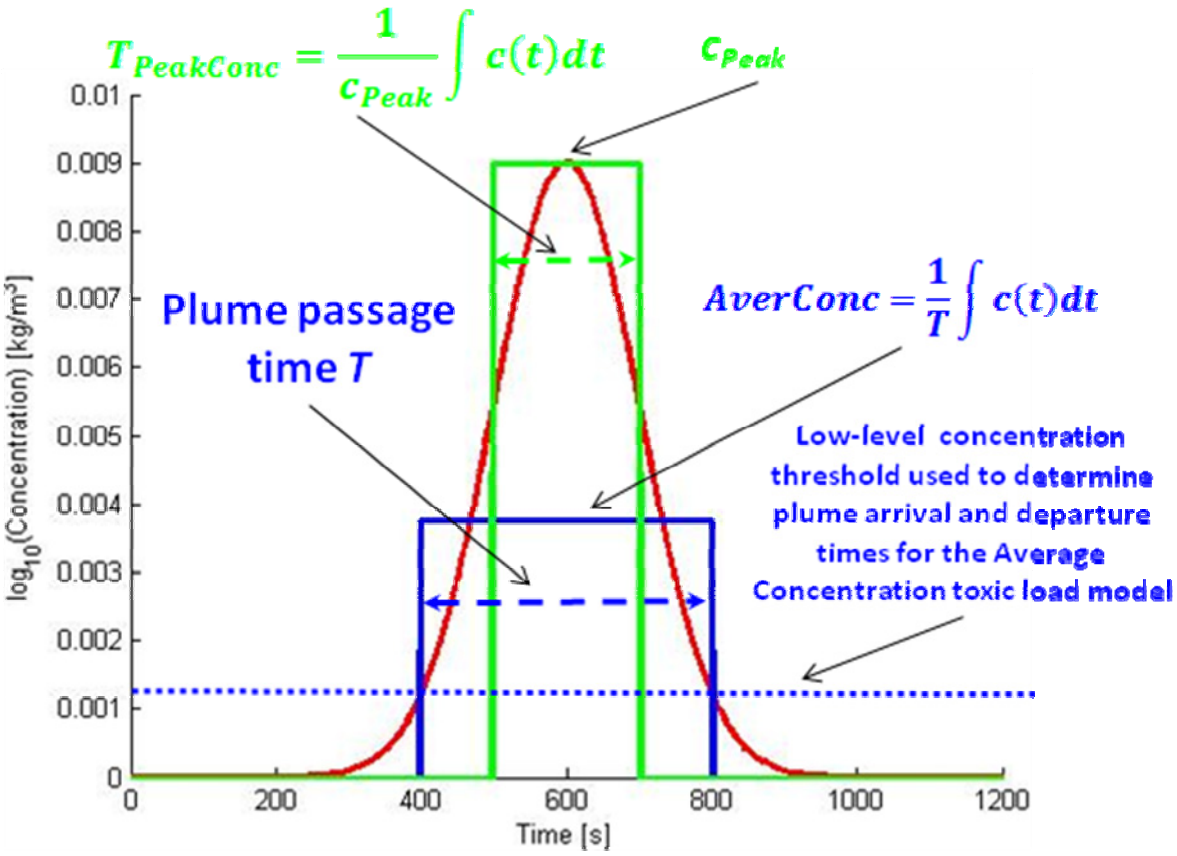

Figure 3. Notional comparison of the Average Concentration and Peak Concentration toxic load models.

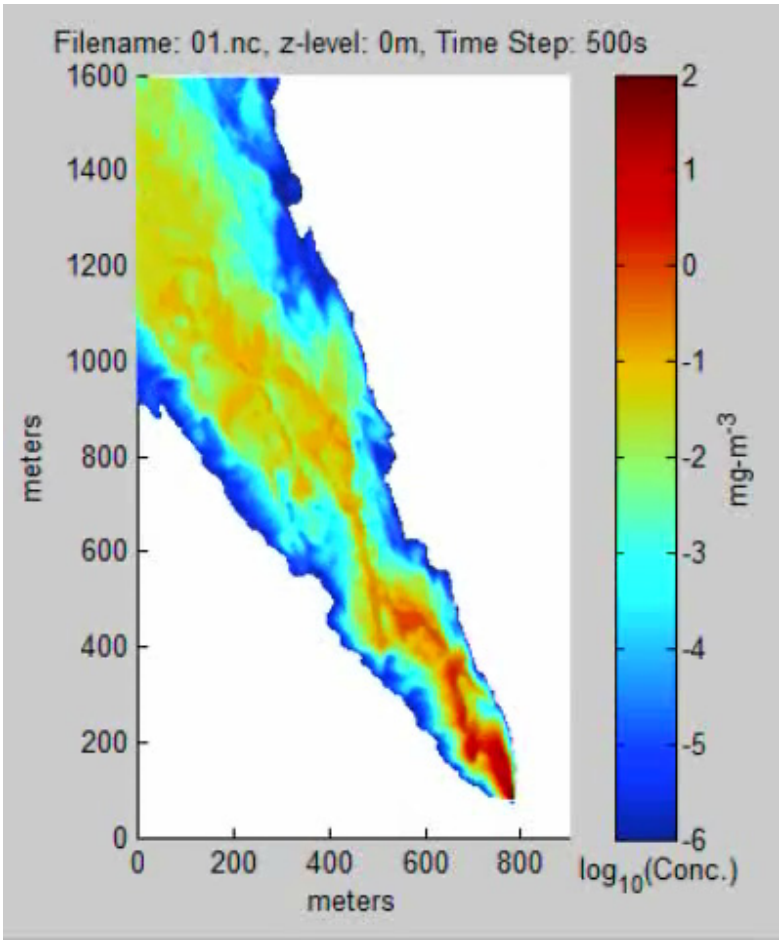

Figure 4. Sample concentration field at 500 seconds for an individual realization of FFT 07 Trial 54 produced by VTHREAT.

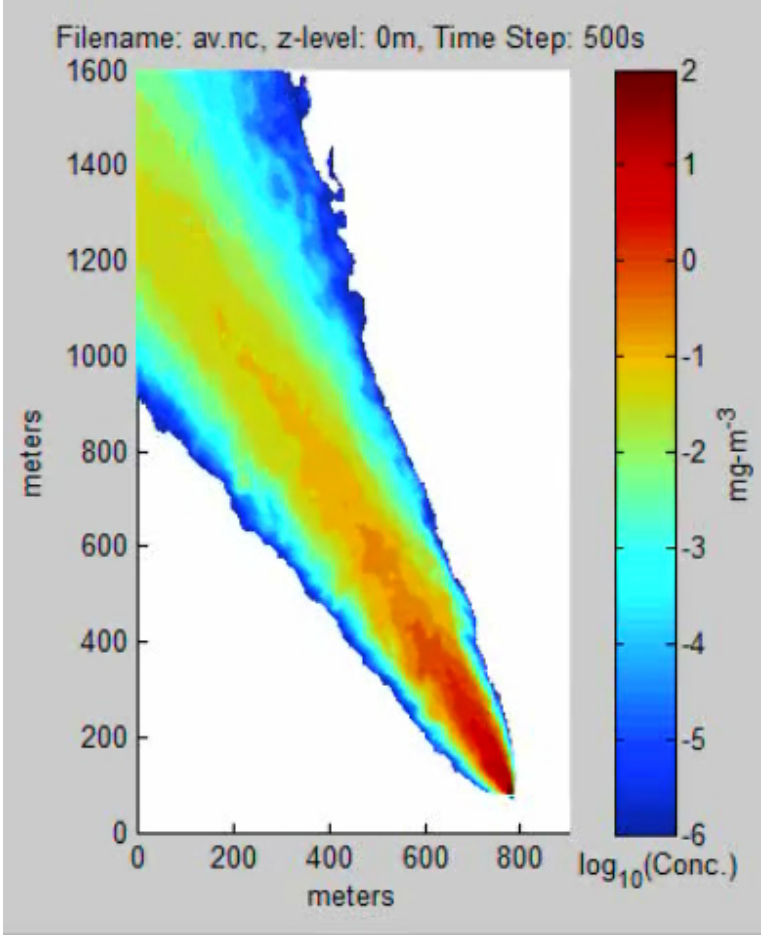

Figure 5. Calculated ensemble mean concentration field at 500 seconds using a point-to-point average over 20 individual realizations of FFT 07 Trial 54 produced by VTHREAT.

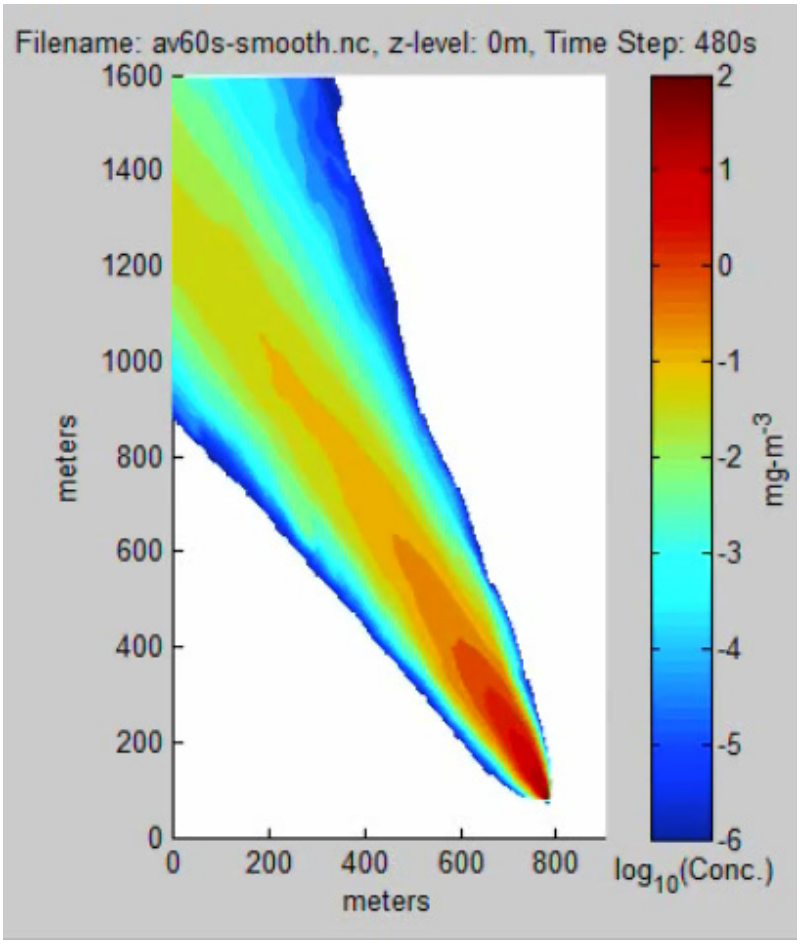

Figure 6. Calculated ensemble mean concentration field at 500 seconds using a point-to-point average over 20 individual realizations of FFT 07 Trial 54 produced by VTHREAT, followed by applying a 60-second running window average. The resulting plume is much smoother than the plume shown in Figure 5, which used an identical procedure for constructing the ensemble average but did not apply additional running window time average.

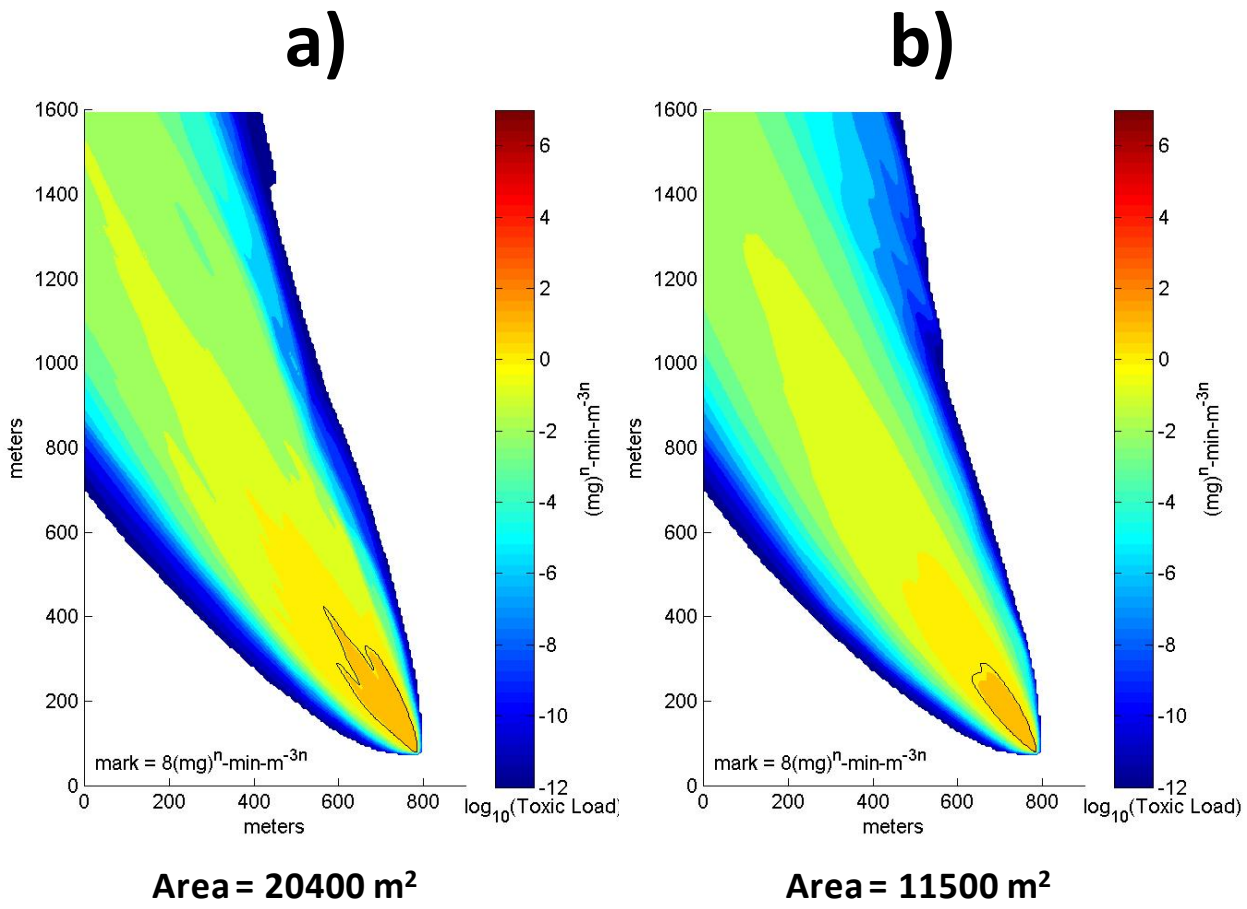

Figure 7. Toxic load contours at 5 meters above ground level calculated using the Integrated Concentration toxic load model with n = 1.5. Panel a) shows toxic load contours for a single realization of the plume. Panel b) shows toxic load contours calculated from an estimate of the ensemble-average concentration field, where the ensemble average was constructed using point-to-point averaging over 20 individual concentration realizations followed by applying a 60-second running window average. The toxic load contour at 8 mg^n-min-m^{-3n} is shown in black; the area enclosed by this contour is shown below the panel.

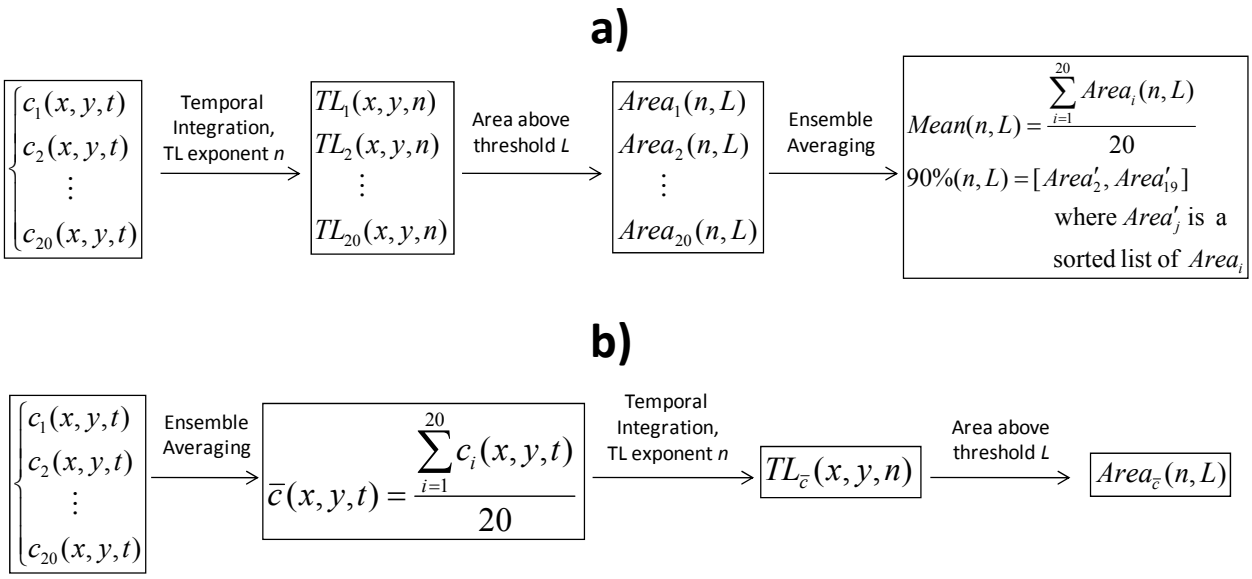

Figure 8. Procedure for calculation comparison metrics from individual plume realizations and from the ensemble average plume. Panel a) illustrates the calculation of metrics based on individual plume realizations, while panel b) illustrates the calculation of metrics based on the ensemble mean plume. Here, $c_i(x,y,t)$ denotes the concentration field for realization i as a function of a horizontal slice (x,y) at a fixed height (e.g., at 5 meters above ground level) and time t, $TL_i(x,y,n)$ denotes the toxic load field for realization i, $Area_i(n,L)$ denotes the area where the toxic load exceeds some threshold L for realization i. Similarly, variables with the subscript $\bar{c}$ denote steps used to calculate metrics based on the ensemble average plume. We would like to note that for the actual release of hazardous materials into the atmosphere, individual people would be expected to be exposed to concentration realizations similar to the individual realizations (including fluctuations) predicted by VTHREAT, and not to the ensemble average plume, which is the quantity that is predicted by the majority of AT&D models in use today.

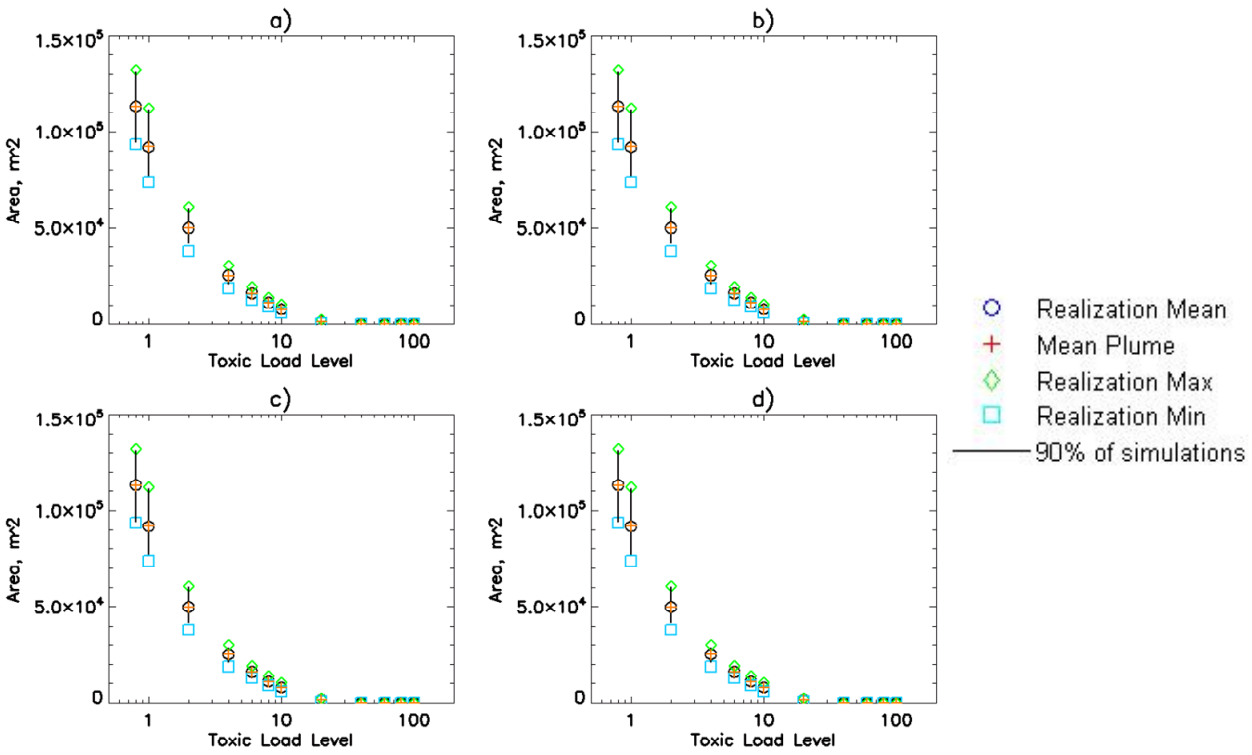

Figure 9. Area exceeding a threshold toxic load as a function of the threshold level for toxic load exponent n = 1. Panel a) shows results from the Average Concentration toxic load model; panel b) shows results from the Integrated Concentration toxic load model, panel c) shows results from the Peak Concentration toxic load model, and panel d) shows results from the Concentration Intensity toxic load model. The realization mean, denoted by black circles, corresponds to the average taken over 20 areas derived from individual realizations of the plume; the realization maximum, denoted by light green diamonds, corresponds to the largest area-above-threshold among the individual plume realizations; the realization minimum, denoted by light blue squares, correspond to the smallest area-above-threshold among the individual plume realizations; and the vertical black line denotes the span of areas-above-threshold for the middle 90% of values derived from individual plume realizations. The brown pluses denote the areas exceeding a toxic load threshold calculated from the estimated ensemble mean plume.

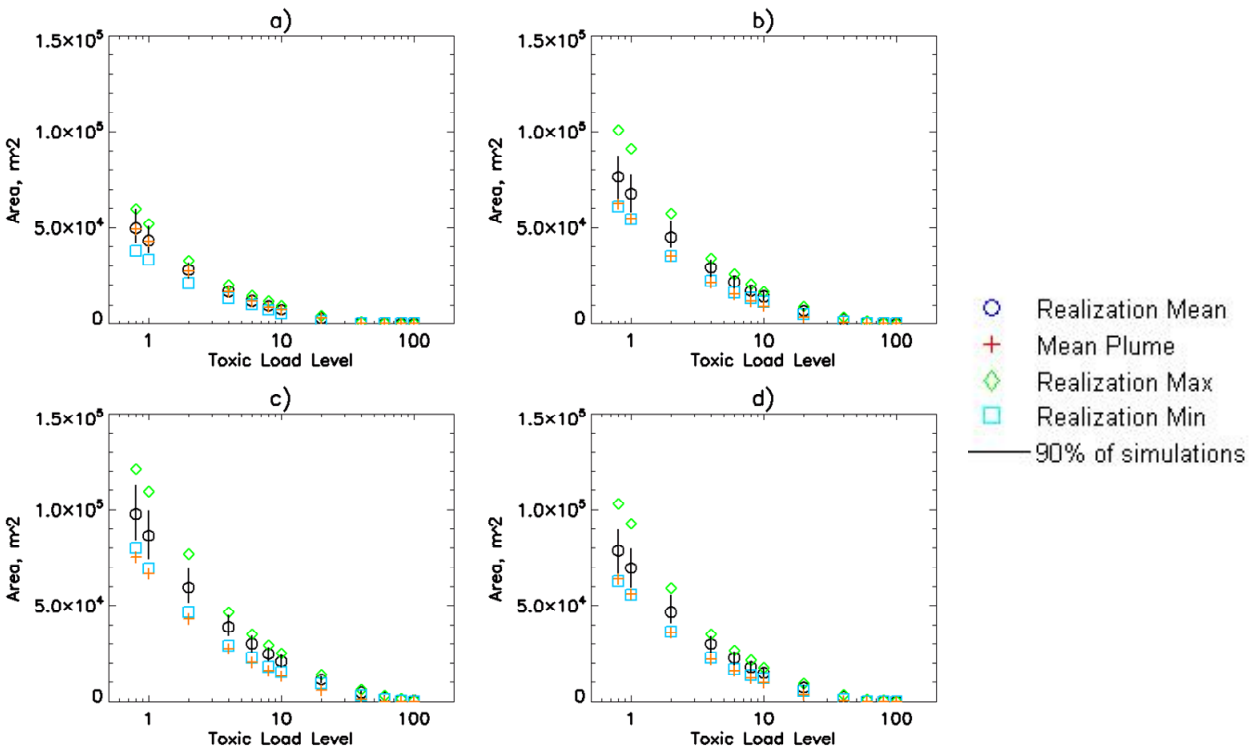

Figure 10. Area exceeding a threshold toxic load as a function of the threshold level for toxic load exponent n = 1.5. Panel a) shows results from the Average Concentration toxic load model, panel b) shows results from the Integrated Concentration toxic load model, panel c) shows results from the Peak Concentration toxic load model, and panel d) shows results from the Concentration Intensity toxic load model.

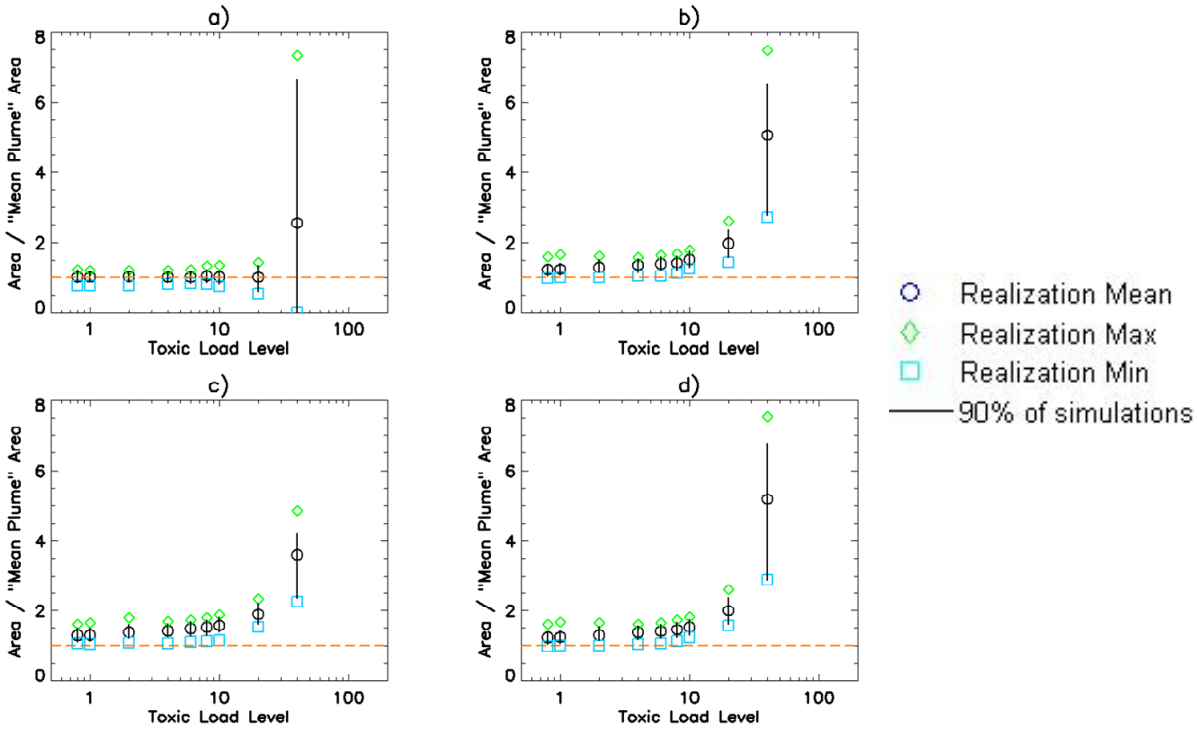

Figure 11. Ratio of the area exceeding a threshold toxic load for individual plume realizations to the area exceeding the threshold for the estimated ensemble mean plume as a function of the threshold level for toxic load exponent n = 1.5. Panel a) shows results from the Average Concentration toxic load model, panel b) shows results from the Integrated Concentration toxic load model, panel c) shows results from the Peak Concentration toxic load model, and panel d) shows results from the Concentration Intensity toxic load model. The brown dashed line indicates where the area ratio equals 1 (i.e., when the toxic load hazard area for an individual realization equals the hazard area for the estimated ensemble mean plume).

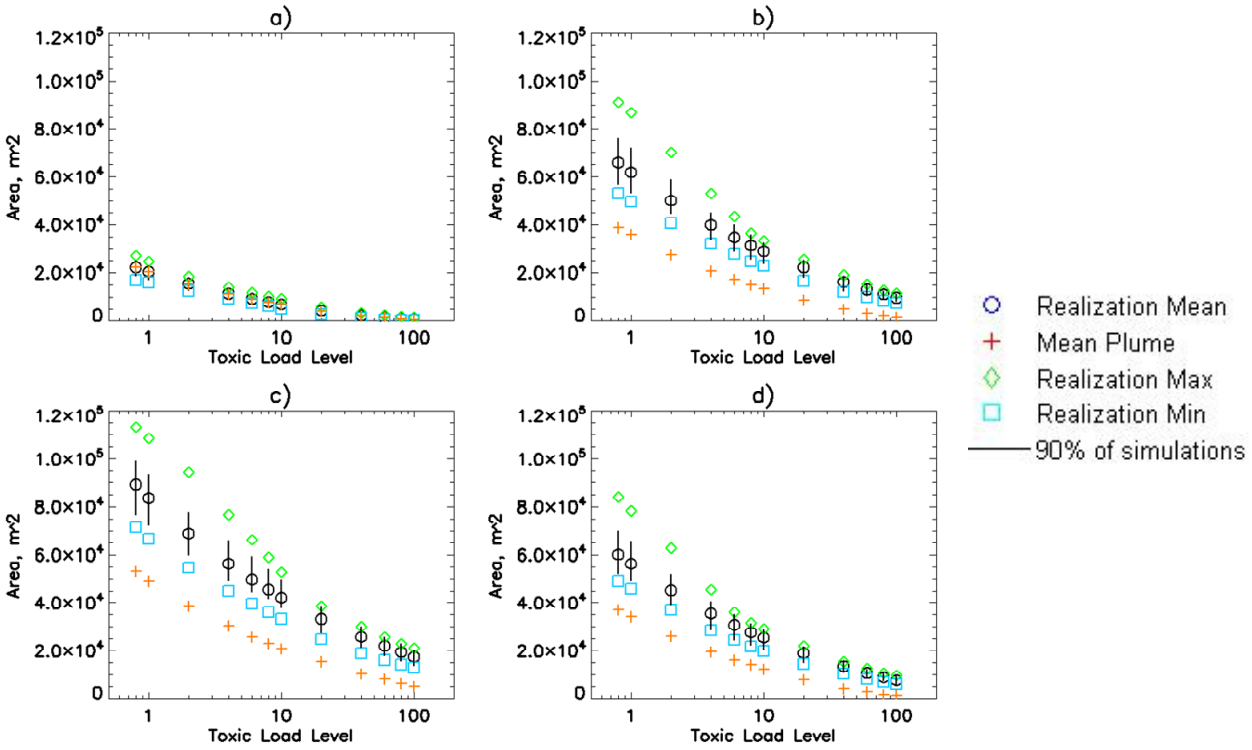

Figure 12. Area exceeding a threshold toxic load as a function of the threshold level for toxic load exponent n = 2.75. Panel a) shows results from the Average Concentration toxic load model, panel b) shows results from the Integrated Concentration toxic load model, panel c) shows results from the Peak Concentration toxic load model, and panel d) shows results from the Concentration Intensity toxic load model.

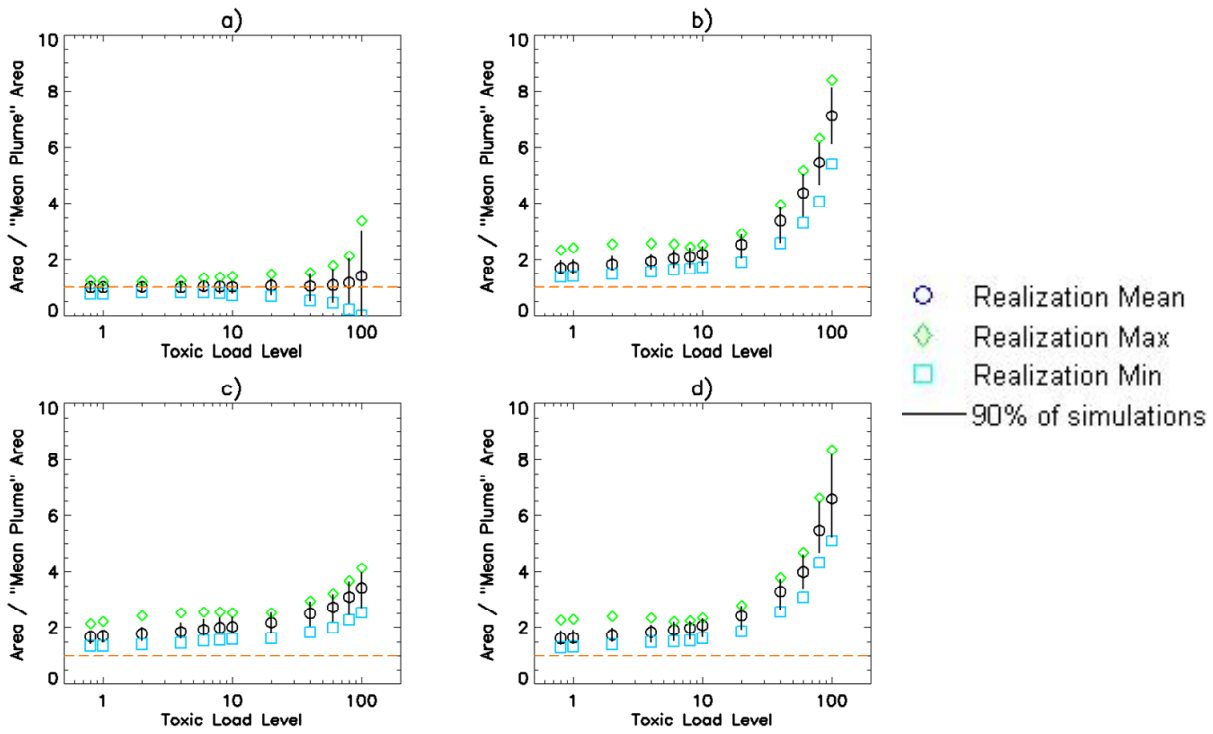

Figure 13. Ratio of the area exceeding a threshold toxic load for individual plume realizations to the area exceeding the threshold for the estimated ensemble mean plume as a function of the threshold level for toxic load exponent n = 2.75. Panel a) shows results from the Average Concentration toxic load model, panel b) shows results from the Integrated Concentration toxic load model, panel c) shows results from the Peak Concentration toxic load model, and panel d) shows results from the Concentration Intensity toxic load model.

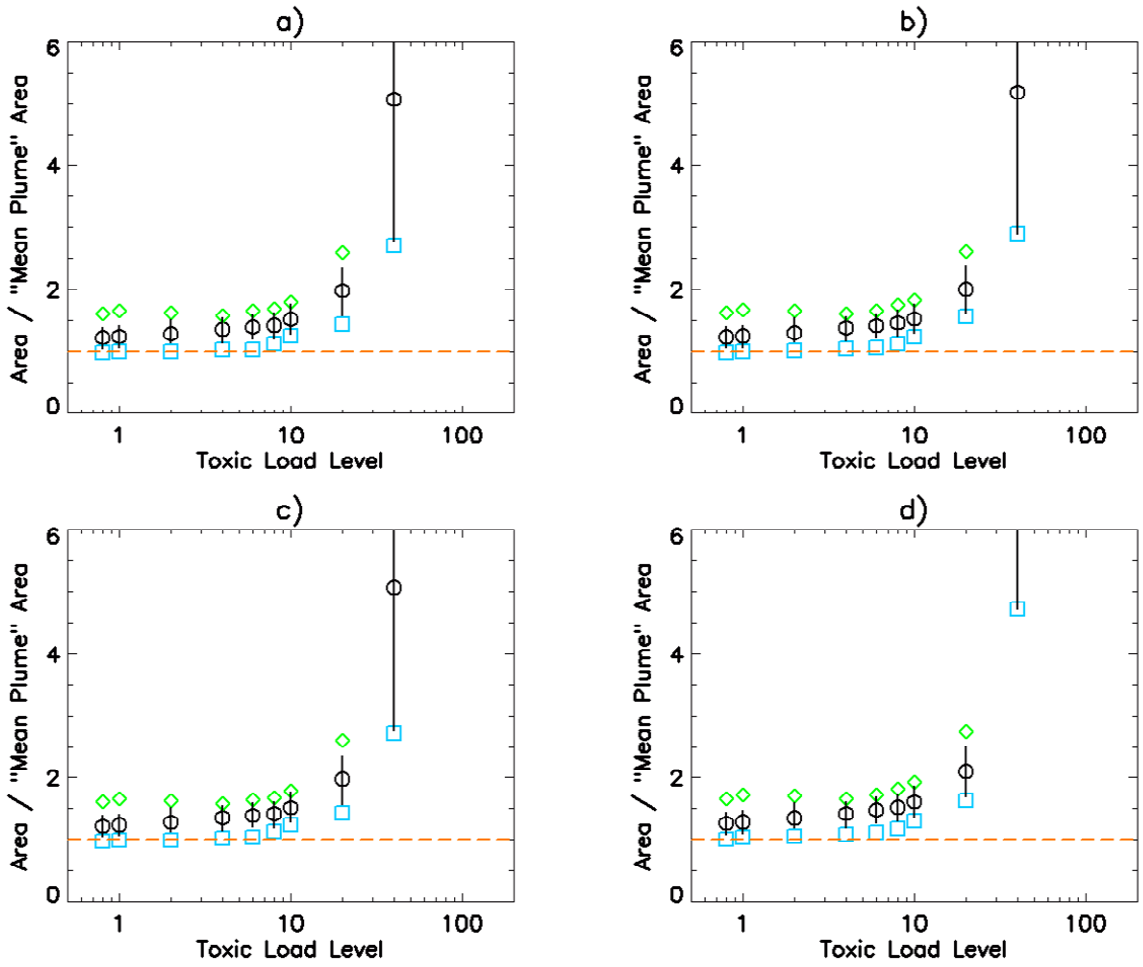

Figure 14. Comparison of the toxic load area ratio as a function of toxic load threshold calculated by two methods for estimating the ensemble mean plume for toxic load exponent n = 1. The toxic load area ratio is the ratio of the area exceeding a threshold toxic load for individual plume realizations to the area exceeding the threshold for the ensemble mean plume. The results from two toxic load models are compared. Panel a) shows results from the Integrated Concentration toxic load model when the ensemble mean plume is estimated by point-to-point averaging in both space and time over 20 individual plume realizations, panel b) shows results from the Concentration Intensity toxic load model when the ensemble mean plume is estimated by point-to-point averaging in both space and time over 20 individual plume realizations, panel c) shows results from the Integrated Concentration toxic load when an additional 60-second running-window time average is applied to the estimated ensemble mean plume, and panel d) shows results from the Concentration Intensity toxic load when an additional 60-second running-window time average is applied to the estimated ensemble mean plume.